Nanoscale Advances

Accepted Manuscript

This article can be cited before page numbers have been issued, to do this please use: S. Ghosh, R. N. Ambade, R. Ram, K. C. Barick, A. Guleria, S. C. Sharma, M. Nayak, A. Kunwar, K. Bhattacharyya and R. Chakravarty, *Nanoscale Adv.*, 2026, DOI: 10.1039/D6NA00347H.

ROYAL SOCIETY OF CHEMISTRY

rsc.li/nanoscale-advances

Nanoscale Advances

View Article Online
DOI: 10.1039/D6NA00347H

COMMUNICATION

Closing the Loop in Nanotheranostics: From ^{124}I Separation to Intrinsically Radiolabeled Platinum Nanoparticles for Potential PET/CT-Guided Photothermal Therapy

Sanchita Ghosh,[a,b] Rajwardhan N. Ambade,[a] Ramu Ram,[a] Kanhu C Barick,[c,b] Apurav Guleria,[d,b] Suresh Chand Sharma,[e] Minati Nayak,[d,b] Amit Kunwar,[d,b] Kaustava Bhattacharyya,[c,b] Rubel Chakravarty[a,b,*]

Closing the loop in nanotheranostics, we integrate radionuclide production with functional nanomedicine through mesoporous alumina based radiochemical separation of no-carrier-added (NCA) ^{124}I and its direct incorporation into protein functionalized platinum nanoparticles. The intrinsically radiolabeled [^{124}I]Pt@GA shows high labeling efficiency, excellent stability, quantitative PET imaging, and effective photothermal cancer cell ablation.

Nanotheranostics has emerged as a compelling approach for precision oncology, bringing diagnosis and therapy together within a single platform, especially when combined with quantitative imaging tools such as positron emission tomography (PET).[1-4] Among the available PET radionuclides, iodine-124 (^{124}I) is particularly well suited for tracking nanoparticle biodistribution because of its relatively long half-life.[5-9] However, its broader use has been limited by challenges in both radiochemical separation and integration with nanomaterials. Conventionally, ^{124}I is recovered from irradiated targets by dry distillation, a method that is technically demanding and requires specialized infrastructure.[10, 11] In contrast, mesoporous alumina-based chromatography offers a simpler and more robust alternative for isolating ^{124}I under milder conditions, with clear potential for direct nanoparticle labeling.[12, 13] Despite these advances, a coherent strategy that directly connects radionuclide separation with functional nanotheranostic design for PET-guided photothermal therapy is still lacking. Conventionally, radionuclide production, radiochemical purification, nanoparticle synthesis, and radiolabeling are performed as separate and sequential operations, often requiring additional processing steps and repeated optimization. Such compartmentalized workflows increase complexity and can impede efficient translation of radionuclides into functional nanotheranostic systems.

Here, we address this gap by bringing together radionuclide production, efficient separation, and functional nanoplatform design within a single framework. ^{124}I was produced via the ^{124}Te (p,n) ^{124}I reaction using a natural TeO_2 target under 14 MeV proton irradiation, followed by its isolation using a mesoporous alumina-based chromatographic method developed in this work.[12, 13] By linking isotope production, separation, nanomaterial fabrication, and multimodal imaging-guided therapy within a single workflow, this study closes the loop between radiochemical processing and nanotheranostic design. The separated ^{124}I was then directly incorporated into gum arabic glycoprotein functionalized platinum nanoparticles (Pt@GA NPs) (Figure 1a). This intrinsic radiolabeling approach affords high labeling efficiency while preserving the physicochemical integrity and photothermal properties of the NPs. The resulting system enables quantitative PET imaging alongside effective photothermal therapy, offering a streamlined route from isotope production and separation to image guided treatment.

Mesoporous alumina, prepared via a solid-state mechanochemical route as reported earlier, was employed as the chromatographic medium for ^{124}I separation.[12, 13] The irradiated target was dissolved in 0.1 M NaOH, adjusted to near-neutral pH (~6), and passed through a compact column. Under these conditions, ^{124}I was selectively retained, while other species were removed by washing with water, followed by elution using dilute NaOH (0.01 M) (Figure S1). Gamma spectrometry revealed no detectable extraneous radionuclides (other than that of other iodine radioisotopes produced due to use of natural TeO_2 target) (Figure S2), indicating high

[a] Radiopharmaceuticals Division, Bhabha Atomic Research Centre, Trombay, Mumbai, 400085, India
[b] Homi Bhabha National Institute, Anushaktinagar, Mumbai, 400094, India
[c] Chemistry Division, Bhabha Atomic Research Centre, Trombay, Mumbai, 400085, India
[d] Radiation and Photochemistry Division, Bhabha Atomic Research Centre, Trombay, Mumbai, 400085, India
[e] Nuclear Physics Division, Bhabha Atomic Research Centre, Trombay, Mumbai, 400085, India

View Article Online DOI: 10.1039/D6NA00347H

radionuclidic purity. Complementary ICP-AES analysis of the decayed fraction showed Te levels below 0.01 ppm, further confirming the suitability of the isolated ^{124}I for subsequent radiopharmaceutical applications.

Protein functionalized Pt NPs were prepared by reducing chloroplatinic acid in the presence of gum arabic, resulting in a stable aqueous dispersion. The particles showed an average hydrodynamic size of 22.06 ± 0.15 nm with a low polydispersity index (PDI) (Figure 1b), while TEM images revealed smaller, quasi-spherical Pt cores of 4.8 ± 1.4 nm (Figure 1c&d). XRD analysis confirmed the formation of crystalline Pt with a face centred cubic structure (Figure S5), and XPS measurements indicated that platinum is predominantly present in the metallic state,[14, 15] along with surface functionalities associated with the gum arabic coating (Figure S8) (details is given in SI). The presence of gum arabic helps maintain colloidal stability and improves biocompatibility, making the nanoplatform suitable for subsequent biological and therapeutic studies.

The photothermal performance of Pt@GA NPs was evaluated under 808 nm laser irradiation at different concentrations and power densities. A rapid increase in temperature was observed for the NPs, with concentrations of 0.5 and 1.0 mg/mL reaching the therapeutic window (~42–44 °C) within a few minutes, while lower concentrations showed a more modest response (Figure 2a). In contrast, deionized water under identical conditions exhibited only a minimal temperature rise, confirming that the heating originates from the NPs (Figure S10).

The temperature increase depended on both the concentration of NPs and laser power, with higher power leading to faster heating (Figure 2b). Importantly, the Pt@GA NPs maintained consistent heating behaviour over multiple irradiation cycles, indicating good photothermal stability (Figure 2c). The heating capability 0.5 mg/mL of Pt@GA NPs was also confirmed by the colour change observed in the IR thermograms (Figure 2d).Together, these results show that the Pt@GA NPs system can efficiently convert near-infrared light into heat in a controlled and reproducible manner.

The biological response of Pt@GA NPs was evaluated in A549 cells to assess both cell viability and photothermal therapeutic effect. The NPs alone showed minimal cytotoxicity, with cell viability remaining above 90% even at higher concentrations after 48 h incubation, indicating good biocompatibility (Figure S12a). In contrast, upon exposure to 808 nm laser irradiation, a marked decrease in cell viability was observed, demonstrating a clear photothermal effect (Figure S12b). This response was

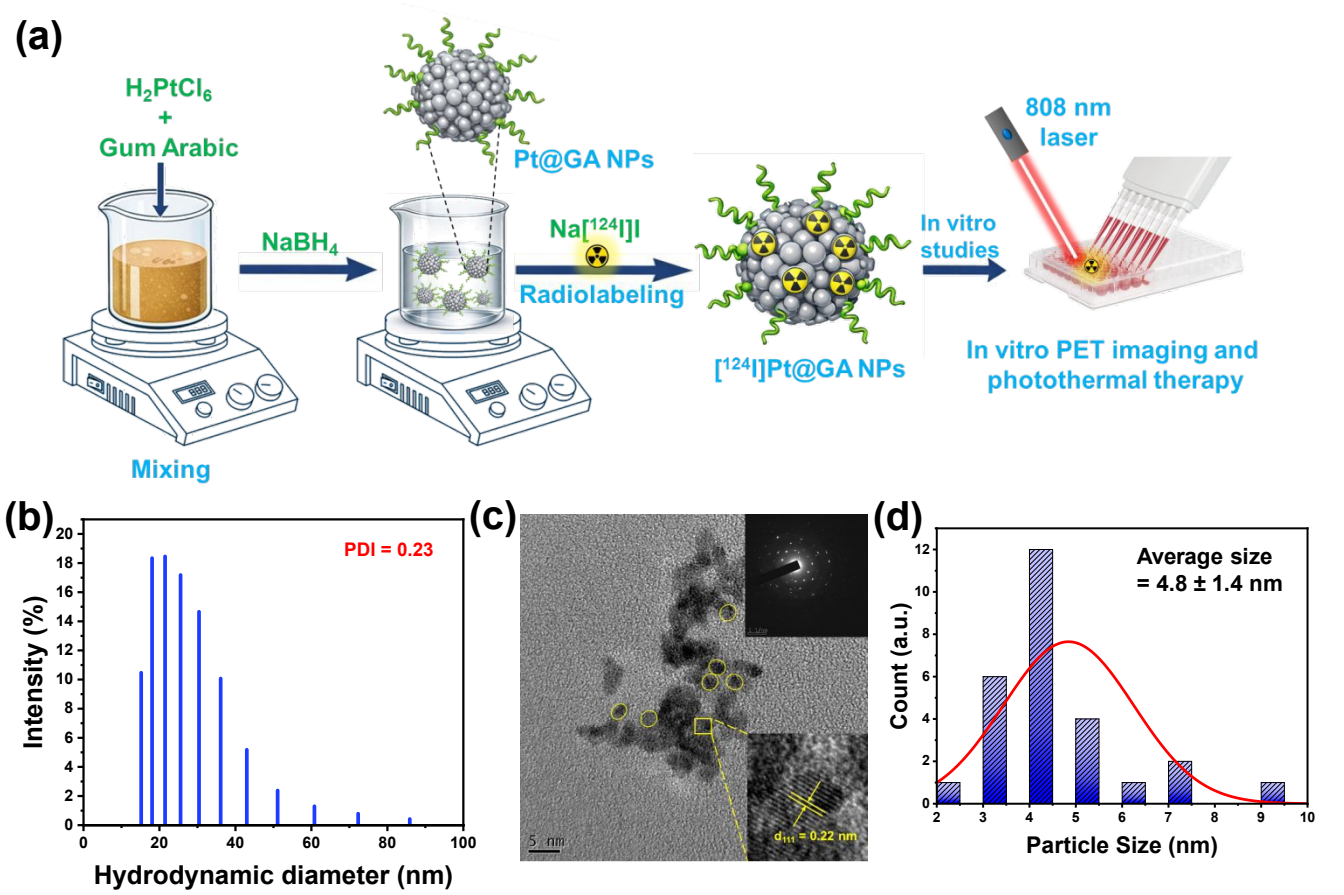

Figure 1 a) Schematic illustration of synthesis of Pt@GA NPs followed by radiolabeling with ^{124}I having potential for PET guided PTT. b) Particle size distribution plot of Pt@GA NPs from DLS. c) HRTEM image of Pt@GA NPs. The insets of the image display the SAED pattern and a magnified view of the Pt@GA NPs. d) Particle size distribution plot of Pt@GA NPs from TEM.

View Article Online
DOI: 10.1039/D6NA00347H

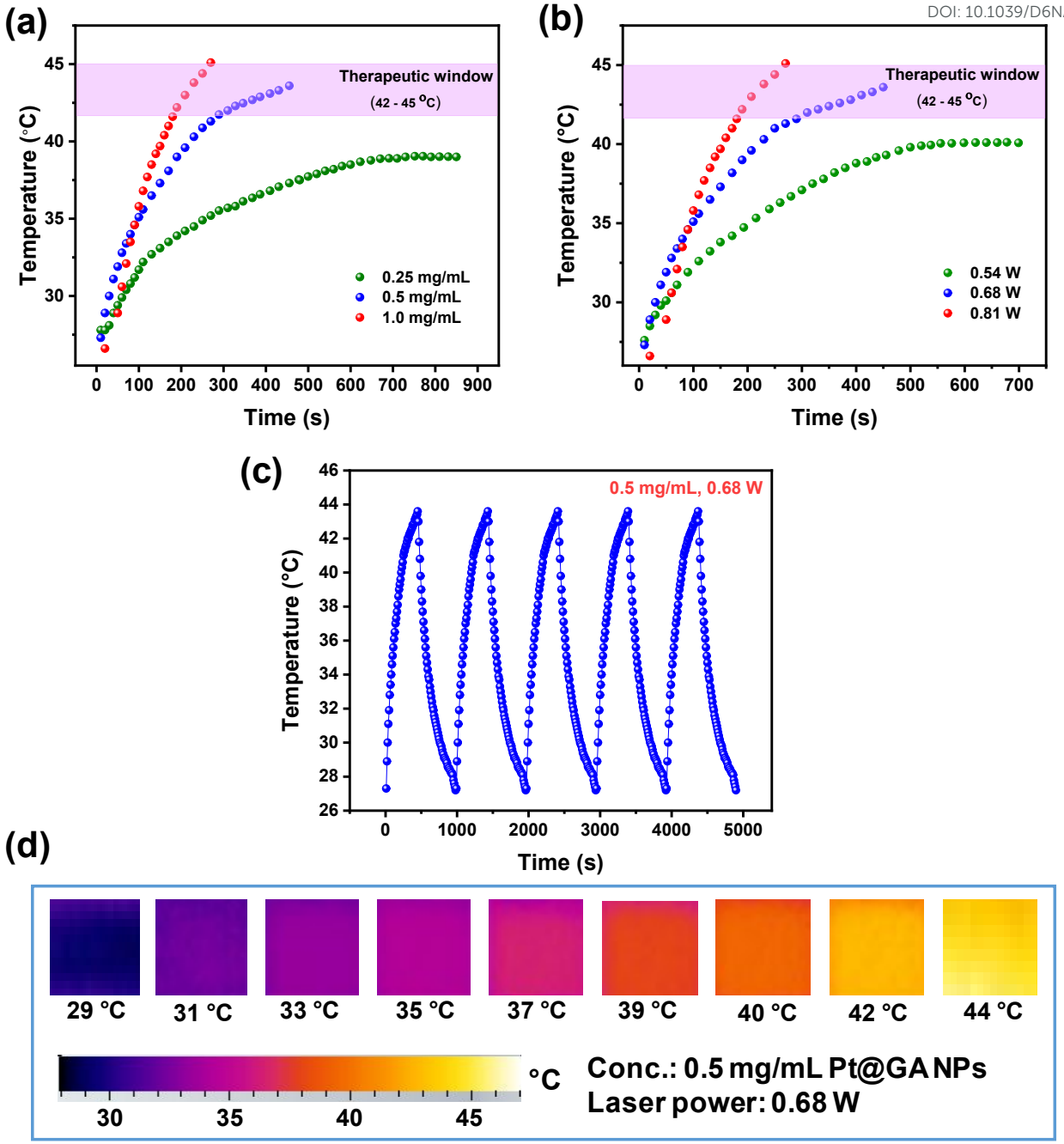

Figure 2 a) Photothermal curves of Pt@GA NPs at different concentrations under 808 nm laser irradiation at power of 0.68 W. b) Photothermal curves of 0.5 mg/mL of Pt@GA NPs at different power of 808 nm laser. c) Recycling heating capability of 0.5 mg/mL Pt@GA NPs at power of 0.68 W. d) IR thermograms of 0.5 mg/mL of Pt@GA NPs solution showing increase in temperature under 808 nm laser irradiation at 0.68 W power.

concentration dependent, with higher concentrations of NPs leading to greater cell death under irradiation. Microscopy images further supported these findings, showing noticeable changes in cell morphology and reduced cell density only in the groups treated with both Pt@GA NPs and laser (Figure S12c). Cells treated with NPs alone or laser alone largely retained their normal morphology. Together, these results confirm that Pt@GA NPs are well tolerated under dark conditions but become effective therapeutic agents upon near-infrared irradiation. While the present biological evaluations establish the efficacy of the Pt@GA NPs as photothermal agents, more detailed mechanistic studies on the various cell death pathways will be undertaken in future work to elucidate the specific cellular pathways involved in treatment-induced cell death.

With a stable and functionally active nanoplatform in hand, we next examined the radiolabeling with ^{124}I. The strong affinity of iodide for noble metal surfaces enabled direct labeling of Pt@GA NPs without additional chelators. Iodide formed stable Pt–I bonds through chemisorption on the platinum surface by simple incubation of the NPs with the separated ^{124}I, with radiochemical yields consistently above 99% as confirmed by size exclusion chromatography (Figure S13). Consistent with

this, The resulting [^{124}I]Pt@GA NPs showed good stability in both phosphate buffered saline and human serum, retaining more than 94% of the activity over 7 days, suggesting a strong association of ^{124}I with the surface of NPs (Figure S14).

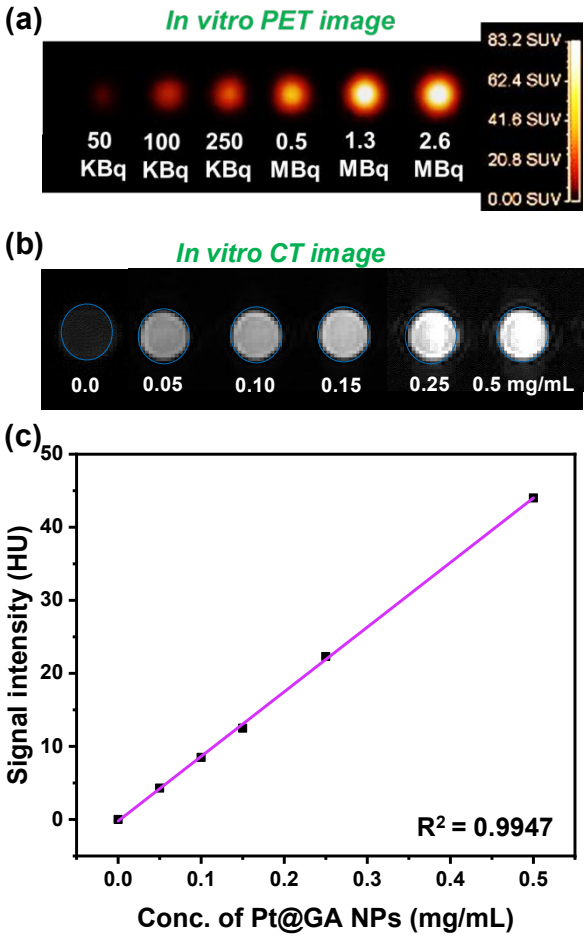

Figure 3 a) In vitro PET images of [^{124}I]Pt@GA NPs at different activity of ^{124}I. b) CT images of Pt@GA NPs at varying concentrations where water was used as the control. c) Plot of mass concentration versus Hounsfield units (HU) demonstrates a linear relationship, indicating concentration dependent X-ray attenuation.

In vitro PET imaging provided a clear and quantifiable signal from the radiolabeled NPs across different activity levels (Figure 3a). In parallel, CT imaging showed a concentration dependent increase in contrast, consistent with the high X-ray attenuation of Pt (Figure 3b&3c). These observations collectively imply that [^{124}I]Pt@GA NPs offer a dual PET/CT imaging platform, without compromising their photothermal therapeutic potential.

The combined outcomes of this research demonstrate a cohesive strategy that bridges radionuclide production and separation processes with the engineering and application of functional nanomaterials. The use of mesoporous alumina enables a straightforward and mild approach for obtaining high-purity ^{124}I, which can be directly integrated with Pt@GA NPs without additional modification. At the same time, the NPs retain their photothermal properties and show good biocompatibility, while also supporting stable radiolabeling for quantitative PET imaging. The additional CT contrast further extends the system toward multimodal imaging. Rather than treating these steps independently, this work brings them into a single workflow, offering a practical path from isotope generation to image-guided photothermal therapy. More broadly, this approach highlights how radiochemical processing can be considered as part of nanomaterial design and may be extended to other radionuclides and nanoplatforms.

CRediT authorship contribution statement

Sanchita Ghosh: Writing – original draft, Validation, Formal analysis, Data curation, Investigation. Rajwardhan N. Ambade: Data curation. Ramu Ram: Data curation. Kanhu C Barick: Data curation, Formal analysis. Apurav Guleria: Data curation, Formal analysis. Suresh Chand Sharma: Data curation. Minati Nayak: Data curation. Amit Kunwar: Data curation, Formal analysis. Kaustava Bhattacharya: Data curation, Formal analysis. Rubel Chakravarty: Writing – review & editing, Supervision, Project administration, Conceptualization.

Conflicts of interest

There are no conflicts to declare.

Data availability

The data supporting this article have been included as part of the supplementary information (SI).

Acknowledgements

The authors acknowledge that research at Bhabha Atomic Research Centre (BARC) is part of the ongoing activities of the Department of Atomic Energy (DAE), Government of India, and is fully supported through internal funding. The authors sincerely thank Dr. Y. K. Bhardwaj (Associate Director, Radiochemistry and Isotope Group, BARC), Dr. T. Das (Head, Radiopharmaceuticals Division, BARC), Mr. N.S. Baghel (Head, Radiation Medicine Centre (G), BARC), Dr. N. Choudhury (Head, Chemistry Division, BARC), Dr. V. Sudarsan (Head, Radiation and Photochemistry Division, BARC) and Dr. S. Chakraborty (Head, Radiochemicals Section, Radiopharmaceuticals Division, BARC) for their constant encouragement and support. The authors also thank the staff members of the BARC–TIFR Pelletron facility for their assistance in the irradiation of the target. The authors acknowledge the Sophisticated Analytical Instrument Facility (SAIF), Indian Institute of Technology Bombay, for providing TEM imaging support.

References

1. W. Hu, X. Wang, Y. Feng, Y. Wang, H. Wang, L. Feng, B. Yang, Y. Gao, D. Jiang and M. Li, ACS Applied Materials & Interfaces, 2025, 17, 56704-56718.
2. J. Sun, L. Li, W. Cai, A. Chen and R. Zhang, ACS Applied Bio Materials, 2021, 4, 5312-5323.
3. N. Priyadarshni, R. Singh and M. K. Mishra, Cancer letters, 2024, 587, 216710.
4. M. A. B. Saddique, M. D. Amjad, H. Tahir and K. Sajid, in *Nanotheranostics and Precision Oncology*, Elsevier, 2026, pp. 431-462.

View Article Online
DOI: 10.1039/D6NA00347H

5. V. V. Belov, A. A. Bonab, A. J. Fischman, M. Heartlein, P. Calias and M. I. Papisov, Molecular pharmaceutics, 2011, 8, 736-747.
6. J. Y. Lee and J. H. Park, New Journal of Chemistry, 2025, 49, 19472-19478.
7. C. Mamat, 2025.
8. D. Kersting, W. Jentzen, P. Fragoso Costa, M. Sraieb, P. Sandach, L. Umutlu, M. Conti, F. Zarrad, C. Rischpler, W. P. Fendler, K. Herrmann and M. Weber, Sci Rep, 2021, 11, 17477.
9. S. Takyu, H. Ikeda, H. Wakizaka, F. Nishikido, K.-i. Matsumoto, H. Tashima, H. Suzuki, Y. Funaki, H. Watabe and M. Takahashi, Applied Physics Express, 2023, 16, 116001.
10. P. Bzowski, D. Borys, K. Gorczewski, A. Chmura, K. Daszewska, I. Gorczewska, A. Kastelik-Hryniewiecka, M. Szydło, A. d'Amico and M. Sokół, EJNMMI physics, 2022, 9, 41.
11. K. Kumar and A. Ghosh, Molecules, 2021, 26, 414.
12. R. Chakravarty, J. Bahadur, S. Lohar, S. Jadhav, D. Sen and S. Chakraborty, SN Applied Sciences, 2021, 3, 77.
13. R. Chakravarty, J. Bahadur, S. Lohar, H. D. Sarma, D. Sen, R. Mishra, S. Chakraborty and A. Dash, Microporous and Mesoporous Materials, 2019, 287, 271-279.
14. C. He, S. Sankarasubramanian, A. Ells, J. Parrondo, C. Gumeci, M. Kodali, I. Matanovic, A. K. Yadav, K. Bhattacharyya and N. Dale, ACS catalysis, 2021, 11, 7006-7017.
15. D. Tyagi, K. Scholz, S. Varma, K. Bhattacharya, S. Mali, P. Patil and S. Bharadwaj, international journal of hydrogen energy, 2012, 37, 3602-3611.
16. S. Ghosh, D. Banerjee, A. Guleria and R. Chakravarty, Nuclear Medicine and Biology, 2024, 138, 108947.
17. M. P. Soriaga, Chemical Reviews, 1990, 90, 771-793.

View Article Online
DOI: 10.1039/D6NA00347H

Data Availability Statement

The data supporting this article have been included as part of the Supplementary Information.